Aromatic–Histidine Interactions in the Zinc Finger Motif: Structural Inequivalence of Phenylalanine and Tyrosine in the Hydrophobic Core[†,‡]

Alan Jasanoff[§,∥] and Michael A. Weiss[*,§,⊥]

Department of Biological Chemistry and Molecular Pharmacology, Harvard Medical School, Boston, Massachusetts 02115, and Department of Medicine, Massachusetts General Hospital, Boston, Massachusetts 02114

Received August 4, 1992; Revised Manuscript Received November 17, 1992

ABSTRACT: The classical Zn finger (Cys-$X_{2,4}$-Cys-X_3-Phe-X_5-Leu-X_2-His-$X_{3,4}$-His). The phenycontains an aromatic–histidine interaction (underlined) in its hydrophobic core whose importance is suggested by the marked destablization of a Phe → Leu analogue [Mortishire-Smith, R. J., Lee, M. S., Bolinger, L., & Wright, P. E. (1992) *FEBS Lett. 1*, 11–15]. In some Zn finger sequences the central Phe is occasionally replaced by Tyr, and when present, this substitution is generally conserved among species. To investigate whether Tyr would participate in an analogous aromatic–histidine interaction, we have determined the solution structure in a Phe → Tyr mutant domain. Its global fold (the $\beta\beta\alpha$ motif) is similar to that of the Phe domain. Although the variant Tyr maintains edge-to-face packing against the proximal histidine, the phenolic ring is displaced toward solvent. Such displacement increases the solvent accessibility of the Tyr *p*-OH group and reduces steric overlap (and possible electrostatic repulsion) between the Tyr O_ζ and His π electrons. The Tyr analogue exhibits reduced dynamic stability (as indicated by more rapid exchange of amide protons in D_2O) and may alternate in rapid equilibrium between major and minor conformers. Inequivalent Tyr–His and Phe–His interactions are likely to be general features of Zn finger architecture. Molecular modeling based on the Zif268 cocrystal structure [Pavletich, N. P., & Pabo, C. O. (1991) *Science 252*, 809–817] suggests that the variant Tyr *p*-OH group may readily be positioned to contribute a novel hydrogen bond to a DNA phosphate.

The classical Zn finger (Klug & Rhodes, 1987; Berg, 1988, 1990; Gibson et al., 1988) provides a model for studies of metal-dependent peptide folding (Frankel et al., 1987). Its structure (the $\beta\beta\alpha$ motif) has been determined by 2D-NMR[1] spectroscopy (Parraga et al., 1988; Lee et al., 1989a,b; Omichinski et al., 1990, 1992; Neuhaus et al., 1990; Kochoyan et al., 1991a,b) and X-ray crystallography (Pavletich & Pabo, 1991). Sequence determinants of structure and stability have been investigated by peptide mutagenesis (Weiss et al., 1990; Weiss & Keutmann, 1990; Parraga et al., 1991; Kochoyan et al., 1991c,d; Mortishire-Smith et al., 1992; Qian et al., 1992; Jasanoff et al., 1992) and design of a "minimalist" peptide (Michael et al., 1992). These studies probe the informational content of consensus residues in the Zn finger and complement related studies of allowed sequences in other systems (Sandberg & Terwilliger, 1989; Bowie et al., 1990).

Here we focus on the central Phe[2] in the consensus Cys-$X_{2,4}$-Cys-X_3-Phe-X_5-Leu-X_2-His-$X_{3,4}$-His. The phenylalanine ring packs against the proximal histidine (underlined) in the hydrophobic core; this "edge-to-face" interaction may provide an example of a weakly polar interaction (Kochoyan et al., 1991d; Jasanoff et al., 1992). Such interactions arise in general from asymmetric distributions of electronic and nuclear partial charges (Burley & Petsko, 1985, 1986, 1988; Serrano et al., 1991). The particular contribution of aromatic–histidine interactions has recently been emphasized (Loewenthal et al., 1992). In the Zn finger the central phenylalanine projects from the C-terminal β-hairpin into thehydrophobic core (Parraga et al., 1988; Lee et al., 1989b; Omichinski et al., 1990; Klevit et al., 1990; Neuhaus et al., 1990) and appears to stabilize the orientation of the DNA-binding surface (Pavletich & Pabo, 1991). Replacement of Phe by a nonaromatic hydrophobic residue (Leu) leads to marked thermodynamic and structural destabilization (Mortishire-Smith et al., 1992). Variant Tyr-containing sequences are occasionally observed and among species are generally conserved as such in homologous domains; such conservation suggests a local difference in structure and function. Does the variant Tyr also participate in an aromatic–histidine interaction, and if so, what similarities and differences are observed between Phe–His and Tyr–His packing schemes? To address these questions, we have determined the solution structures of related Phe and Tyr analogues. Although the overall $\beta\beta\alpha$ motif is retained in each case, the Tyr phenolic ring is displaced toward solvent, avoiding steric overlap (and possible electrostatic repulsion) between the Tyr O_ζ and His π electrons. We predict that in variant Zn finger–DNA complexes the Tyr *p*-OH will donate a novel hydrogen bond to a DNA phosphate.

MATERIALS AND METHODS

Peptide Synthesis. Peptide sequences are given in Table I. The parent peptide (ZFY-swivel; Jasanoff et al., 1992) has

[†] Supported by the Markey Charitable Trust and a grant from the National Institutes of Health to M.A.W.

[‡] The coordinates of the NMR structures and tables of NMR-based restraints will be deposited in the Brookhaven Data Bank.

[*] Address correspondence to this author at the Department of Biological Chemistry and Molecular Pharmacology at Harvard Medical School.

[§] Harvard Medical School.

[∥] Present address: Department of Chemistry, Cambridge, England.

[⊥] Massachusetts General Hospital.

[1] Abbreviations: Ar, aromatic residue; CD, circular dichroism; DG, distance geometry; DQF-COSY, double-quantum-filtered correlated spectroscopy; NMR, nuclear magnetic resonance; NOE, nuclear Overhauser enhancement; NOESY, NOE spectroscopy; rms, root mean square; rmsd, rms difference; ROESY, rotating frame Overhauser spectroscopy; rp-HPLC, reverse-phase high-performance liquid chromatography; SA, simulated annealing; TOCSY, total correlated spectroscopy; UV, ultraviolet.

[2] Amino acids are designated in the text by three-letter code and in the figures by one-letter code.

0006-2960/93/0432-1423$04.00/0 © 1993 American Chemical Society

the structure Cys-X_2-Cys-X-Tyr10-X-Phe12-X_5-Leu-X_2-His-X_4-His and is related to ZFY-6T (Kochoyan et al., 1991a) by the substitution Ser12Phe. Analogues were synthesized, reduced, and purified by rp-HPLC as described (Weiss et al., 1990). Reduced peptide–Zn^{2+} complexes were lyophilized and stored in an anaerobic N_2 chamber (Coy Laboratories, Inc.).

Circular Dichroism. CD spectra were obtained with an Aviv spectropolarimeter as described (Weiss et al., 1990). CD spectra were obtained in 50 mM Tris-HCl buffer containing 0.1 mM $ZnCl_2$. To obtain unfolding curves, the buffer pH was adjusted in the range 1–9 with 1% acetic acid. Buffers were deoxygenated with N_2 prior to dissolution of peptide.

NMR. Peptides (ca. 10 mg) were dissolved in 0.7 mL of a buffer containing 50 mM deuterated Tris-HCl (pH or pD 6.0; direct meter reading) and 5 mM $ZnCl_2$. 2D-NMR experiments were conducted at 500 MHz and 25 °C (except where noted). DQF-COSY, TOCSY (mixing times 30 and 55 ms), NOESY (mixing times 100 and 200 ms), and ROESY (mixing time 50 ms) experiments were performed by the pure-phase method (States et al., 1982). Data were processed with a combination of exponential and shifted sine-bell window functions in each dimension. The sweep width was 7000–8000 Hz in each dimension; 350–400 t_1 increments were obtained. The 350 × 4K complex data matrices were zero-filled to 4K × 4K (NOESY, ROESY, and TOCSY) or 4K × 8K (DQF-COSY). $^3J_{\alpha N}$ coupling constants were extracted from DQF-COSY cross-peaks in H_2O by spectral simulation as described (Redfield & Dobson, 1990; Smith et al., 1991). Amide proton exchange studies were performed at 25 °C under the same conditions as used for 2D-NMR experiments. The peptide–Zn^{2+} complexes were lyophilized from H_2O solution; the powder was dissolved in D_2O immediately before use. Each time point represents the average of 64 transients (acquisition time 1 min).

NMR-Derived Restraints. NOE and *J*-coupling (dihedral angle) restraints were used for molecular modeling as previously described (Kochoyan et al., 1991a,b; Jasanoff et al., 1992). NOEs were classified as strong (<2.7 Å), medium (<3.4 Å), or weak (<4.3 Å); distance-bound corrections were made for the methyl groups and methylene protons for which stereospecific assignments could not be obtained (Wuthrich, 1986). Dihedral-angle restraints were introduced on the basis of *J*-coupling constants with tolerance of ±40°. Experimental restraints for each analogue are provided as supplementary material. DG/SA calculations were performed with the program DG-II (T. F. Havel, Harvard Medical School). Stereospecific assignment of β-methylene protons (Figure 2) was obtained in selected cases on the basis of intraresidue NOEs and $J_{\alpha\beta}$-coupling constants as described by Wagner et al. (1987).

Hydrogen Bonds. Possible hydrogen bonds in DG/SA structures were calculated with the analysis facility of the program X-PLOR (A. T. Brunger, Yale University). Since the simulated annealing protocol does not contain electrostatic terms or an explicit hydrogen bond potential, possible hydrogen bonds reflect the geometric content of the restraints. We consider as established only those hydrogen bonds that are both consistently predicted by the DG/SA models and correspond to slowly exchanging amide resonances in D_2O. Initial DG/SA structures were calculated in the absence of hydrogen bond restraints; lower bounds equaled the sum of hard-sphere radii. Refined DG/SA structures were calculated, incorporating eight explicit hydrogen bond restraints and revised lower bounds as described by Qian and Weiss (1992).

Table I: Peptide Sequences

analogue	sequence[a]
	1 5 10 15 20 25 30
parent peptide[b]	KTYQCQYCEYRFADSSNLKTHIKTKHSKEK
[Y10F]	KTYQCQYCEFRFADSSNLKTHIKTKHSKEK
[Y10F; F12Y]	KTYQCQYCEFRYADSSNLKTHIKTKHSKEK

[a] Variant aromatic residues at positions 10 and 12 are underlined; motif-specific cysteines and histidines are shown in boldface. [b] The parent peptide is designated ZFY-swivel in Jasanoff et al. (1992) and is related to ZFY-6T (Kochoyan et al., 1991a) by the substitution S12F.

In this protocol peptide hydrogen bonds were introduced as lower and upper bounds on the distance between the amide proton and carbonyl oxygen (1.9–2.5 Å); amide–sulfur hydrogen bonds were introduced as bounds on the distance between the amide proton and sulfur (2.2–2.8 Å). To avoid systematic errors (Akke et al., 1992), lower bounds between amide protons and other possible oxygen acceptors were reduced to 1.9 Å (i.e., 0.4 Å less than the sum of their hard-sphere radii); no upper bounds were imposed.

RESULTS

Overview. The present studies are based on the solution structure of ZFY-swivel (Jasanoff et al., 1992); its sequence and numbering scheme are given in Table I. ZFY-swivel exhibits classical Phe12–His21 edge-to-face packing in its hydrophobic core; an additional aromatic residue, Tyr10, occurs on the surface and is less well-ordered. In the absence of an aromatic residue at position 12, Tyr10 (or, equivalently, Phe10) packs horizontally against His21 (Kochoyan et al., 1991b; Qian & Weiss, 1992). Here we study two analogues of ZFY-swivel, containing successive substitutions [Tyr10Phe] and [Tyr10Phe; Phe12Tyr] (Table I). The latter analogue provides a model of a variant Tyr–His interaction.

Relative pH Stabilities.[3] Far-UV CD spectra obtained in the absence and presence of Zn^{2+} demonstrate in each case metal-dependent peptide folding (data not shown). Because [Tyr10Phe] and [Tyr10Phe; Phe12Tyr] substitutions do not introduce or remove titratable groups in the pH range 2–8, the pH dependence of mean residue ellipticity at 222 nm ($[\theta]_{222}$) may be used to probe relative differences in thermodynamic stability (Weiss & Keutmann, 1991). Unfolding of the parent peptide, [Tyr10Phe], and [Tyr10Phe; Phe12Tyr] occurs with pH midpoints of 4.8, 4.6, and 4.8, respectively (supplementary material). Such similar pH titrations indicate that neither mutation significantly alters overall thermodynamic stability. The first mutation is slightly stabilizing relative to the parent peptide, and the second mutation is slightly destablilizing relative to the first analogue.

^{1}H-NMR Studies. In the presence of equimolar Zn^{2+}, ^{1}H-NMR spectra of each analogue exhibit a range of chemical shifts similar to that of the parent peptide (supplementary material). NOESY "fingerprint" regions for the three peptides are shown in Figure 1. Sequential assignment is analogous to that of the parent peptide (Jasanoff et al., 1992). The amide–aromatic region of the NOESY spectrum contains in each case similar d_{NN} and cross-sheet NOEs (supplementary material). Sequential and medium-range NOEs and selected ^3J-coupling constants are shown in schematic form in Figure 2 (the [Tyr10Phe] analogue in panel A and the [Tyr10Phe;

[3] In this paper the term *stability* is used in two senses. *Thermodynamic stability* refers to a free-energy difference between the folded and unfolded states. *Dynamic stability* refers to structural fluctuations within the folded state.

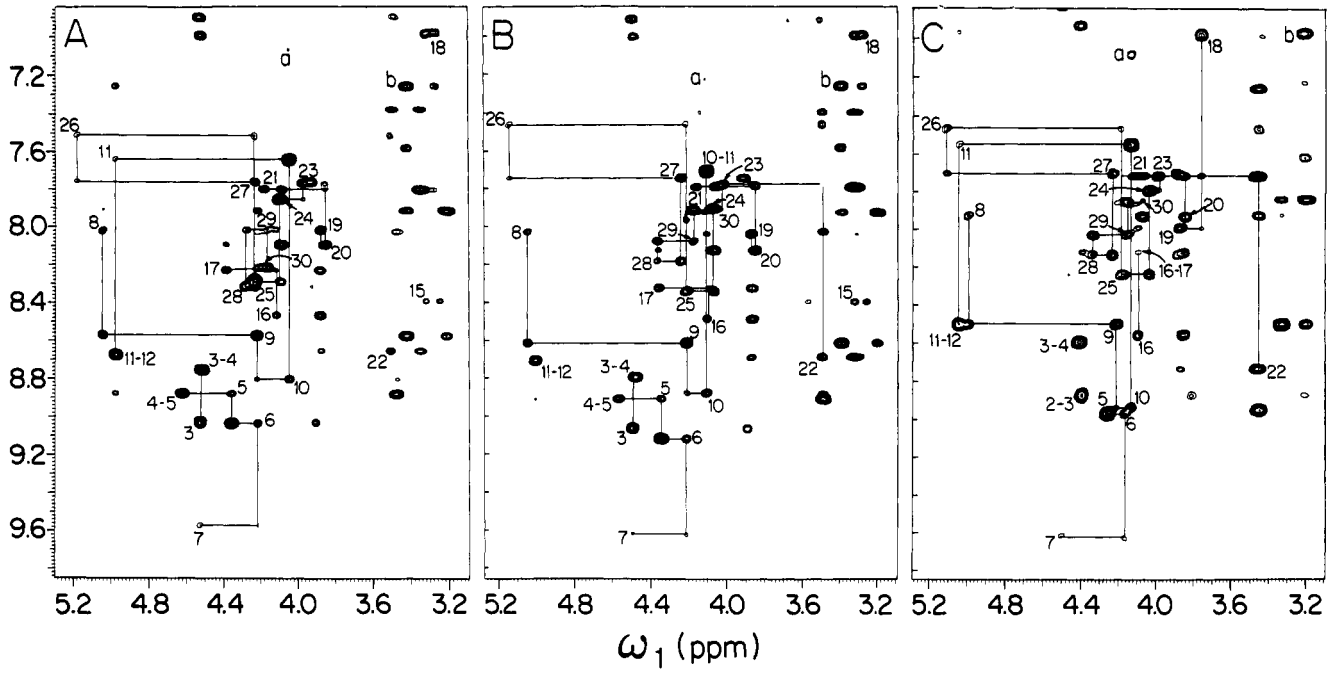

FIGURE 1: Fingerprint regions of NOESY spectra in H_2O of ZFY-swivel (A) and [Tyr10Phe] and [Tyr10Phe; Phe12Tyr] analogues (B and C, respectively). In each panel corresponding intraresidue Ar10 H_δ–H_α and Ar12 H_δ–H_β cross-peaks are labeled a and b.

Phe12Tyr] analogue in panel B). In each case residues 13–15 are not well-defined by sequential NOEs due to rapid amide proton exchange in H_2O; their spin systems were assigned on the basis of side-chain NOEs and the presence of a unique spin system (Ala13). These data demonstrate that the two analogues retain classical $\beta\beta\alpha$ secondary structure. The register of the β-sheet is defined by cross-strand NOEs between residues 2 and 13, 3 and 12, and 4 and 11. The helical segment extends from residues 15 to 26. The configuration of the N-terminal residue of the α-helix, Asp14, is well-defined by stereospecific assignment of its β-resonances and by observation of medium-strength NOEs from its β-resonances to Asn17-NH; its configuration is consistent with formation of an N-cap hydrogen bond (Richardson & Richardson, 1988) between the Asp14 γ-carboxylate and Asn17-NH as discussed elsewhere (Qian & Weiss, 1992). Helical geometry in the His-X_4-His region is nonstandard, as indicated by large $^3J_{HN\alpha}$ coupling constants at positions 25 and 26 (Figure 2A,B; Kochoyan et al., 1992b).

Comparison of ^{1}H-NMR Chemical Shifts. Chemical shifts of assigned resonances in the [Tyr10Phe] and [Tyr10Phe; Phe12Tyr] analogues are given in Tables II and III, respectively. Chemical shifts in the [Tyr10Phe] analogue are essentially identical to those of the parent peptide (Jasanoff et al., 1992); only small differences (less than 0.10 ppm in magnitude) are observed (Table IV, set A). More extensive changes in chemical shift occur in the spectrum of the [Tyr10Phe; Phe12Tyr] analogue (Table IV, set B). Their structural origins are considered below.

Comparison of NOESY Spectra. Packing of the N-terminal β-sheet against the C-terminal α-helix is demonstrated in each case by long-range NOE contacts, including Tyr3–Leu18, Tyr7–Ile22, and Ar12–Leu18 (panels A and B of Figure 3, respectively). These and other interresidue NOEs are summarized in diagonal plots (panels C and D of Figure 2). In the [Tyr10Phe] analogue long-range NOEs from Phe12 are identical to those of the parent peptide, demonstrating that the substitution does not alter the packing of Phe12 in the hydrophobic core. In neither ZFY-swivel nor the [Tyr10Phe] analogue are long-range NOEs observed from the aromatic ring at position 10.

In the [Tyr10Phe; Phe12Tyr] analogue corresponding Tyr12–Leu18 and Tyr12–His21 NOEs establish the presence of a related Tyr–His interaction. Two significant differences are noteworthy: (i) Medium-strength NOEs are observed from the β-protons of Tyr12 to Tyr3-NH, which are not observed in ZFY-swivel or the [Tyr10Phe] analogue. (ii) The [Tyr10Phe; Phe12Tyr] analogue exhibits weak NOEs from the Phe10 meta ring resonance (H_ϵ) to the β-resonances of Tyr12 and the α-resonance of Leu18. Additional weak NOEs are observed at 10 °C from the Phe10 ortho ring resonance (H_δ) to the β-resonances of Cys5 and from the Phe10 para ring resonance (H_ζ) to a methyl resonance of Leu18. Such NOEs are not observed in ZFY-swivel or the [Tyr10Phe] analogue. Distance-geometry calculations (below) indicate that these Phe10 NOEs—which would position its aromatic ring in the hydrophobic core—are inconsistent with the strong long-range NOEs involving Tyr12. The presence of minor, geometrically inconsistent NOEs suggests that the analogue exists in rapid equilibrium (fast exchange) between a major state (in which Tyr12 is internal) and a minor state (in which Phe10 is internal); no doubling of cross-peaks is observed as described in the spectrum of an ADR1 Zn finger (Xu et al., 1991). No NOEs are observed between the F10 and Y12 rings, suggesting that the minor conformer does not contain both rings in its hydrophobic core. The minor conformation may be analogous to that of ZFY-6T, in which Tyr10—in the absence of an aromatic residue at position 12—also projects into the hydrophobic core (Kochoyan et al., 1991a,b).

Slowly Exchanging Amide Resonances. In the parent peptide and the two analogues eight slowly exchanging amide resonances are observed in freshly prepared D_2O solutions (data not shown), assigned in each case to Cys5, Tyr7, Cys8, residue 10, residue 12, Ile22, Lys23, and Thr24. The exchange properties of ZFY-swivel and the [Tyr10Phe] analogue are similar and may be rationalized by inspection of the DG/SA model (Jasanoff et al., 1992). Amide protons of Cys5 and residue 12 participate in cross-sheet hydrogen bonds; amide protons of Ile22, Lys23, and Thr24 participate in helix-related

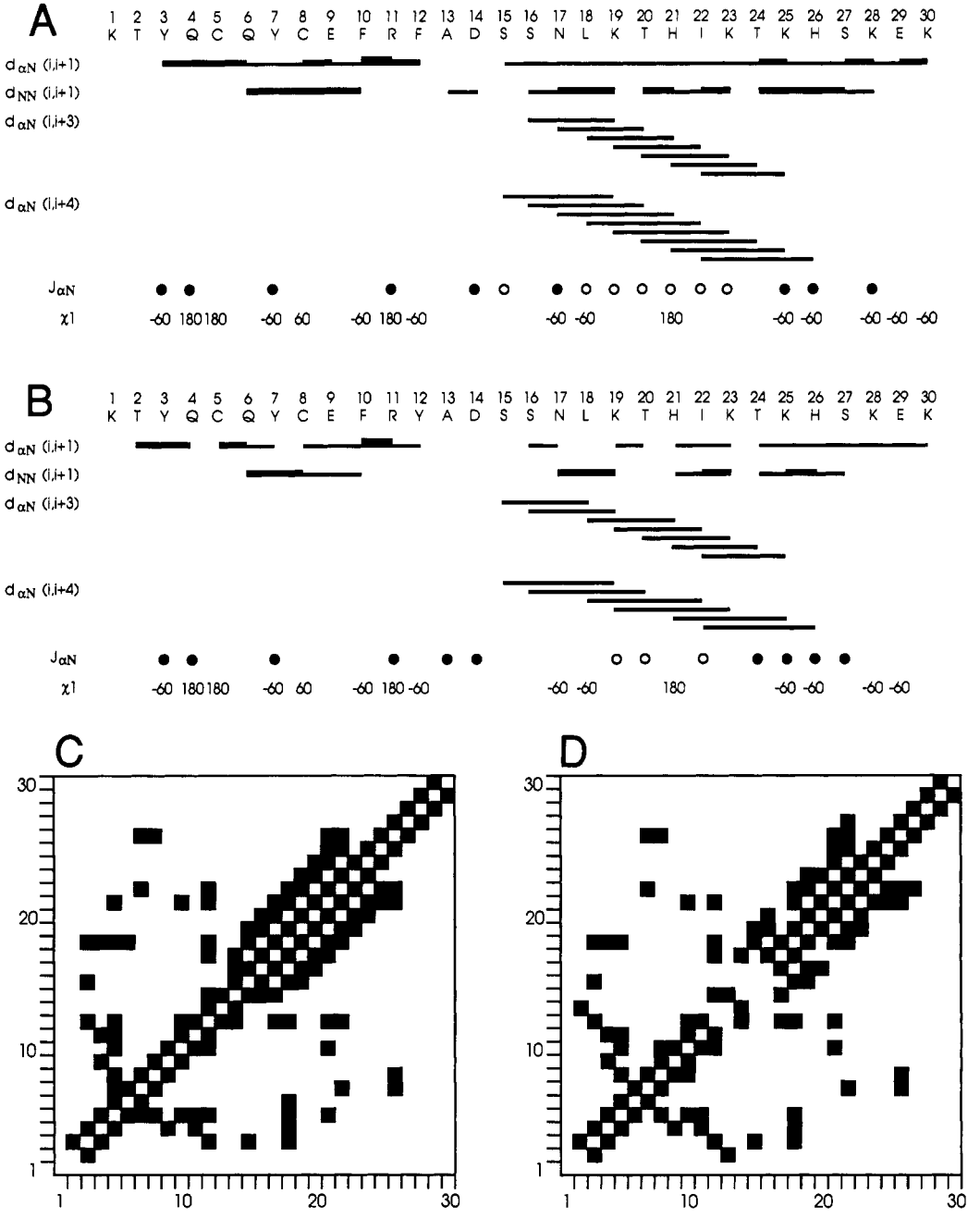

FIGURE 2: (A and B) Summary of sequential and medium-range NOEs for [Tyr10Phe] and [Tyr10Phe; Phe12Tyr] analogues, respectively. Symbols ($d_{\alpha N}$, d_{NN}, etc.) are as defined by Wuthrich (1986). Large and small $^3J_{NH\alpha}$ values are indicated by closed and open circles, respectively; χ^1 values are indicated for residues for which stereospecific assignment of β-resonances was obtained. The absence of a d_{NN} NOE between residues Lys23 and Thr24 is due to limited resolution. (C and D) Diagonal plots of interresidue NOEs observed in [Tyr10Phe] and [Tyr10Phe; Phe12Tyr] analogues, respectively. Differences in the [Tyr10Phe; Phe12Tyr] analogue are due primarily to absence of certain NOEs (at similar signal-to-noise ratios) rather than to an altered pattern of resonance overlap.

hydrogen bonds; the amide proton of residue 10 forms a hydrogen bond with the sulfur of Cys8; and the amide protons of Tyr7 and Cys8 form a bifurcated hydrogen bond to the sulfur of Cys5. This set of inferred hydrogen bonds is essentially as described (Qian & Weiss, 1992); amide–sulfur hydrogen bonds were predicted by Berg (1988).

Rates of amide proton exchange vary from site to site (Figure 4). Of the slowly exchanging subset of amide resonances, the shortest lived are Lys23 and Thr24 in the His-X_4-His site; the longest lived correspond to the two $S_{\gamma i}$–NH_{i+2} amide–sulfur hydrogen bonds (Tyr7 and residue 10; Figure 4). Of the bifurcated $S_{\gamma 5}$ hydrogen bonds, exchange of Cys8-NH is more rapid than that of Tyr7-NH. Asynchrony among sites suggests that structural fluctuations responsible for amide proton exchange are influenced by local features. Unlike the [Tyr10Phe] analogue, the [Tyr10Phe; Phe12Tyr] analogue exhibits more rapid exchange at each site except Cys8-NH (whose exchange rate is similar in the two analogues; see Figure 4) and thus exhibits decreased dynamic stability.

Distance-Geometry Calculations. A summary of restraints used in calculating DG/SA models of the two analogues is provided in Table V; restraint lists are provided as supplementary material. For the [Tyr10Phe; Phe12Tyr] analogue weak nonlocal NOEs from Phe10 were omitted due to geometric inconsistencies (see below). Mean NOE restraint violations in the parent ensemble are 0.011 Å; in the [Tyr10Phe] analogue, 0.012 Å; and in the [Tyr10Phe; Phe12Tyr] analogue, 0.052 Å. The mean violation of dihedral restraints was 1.16° in the [Tyr10Phe; Phe12Tyr] analogue; none occurred in models of the [Tyr10Phe] analogue or parent

Table II: Chemical Shifts of Assigned ^{1}H-NMR Resonances in the [Tyr10Phe] Analogue

residue	chemical shift (ppm)			
	NH	$C^{\alpha}H$	$C^{\beta}H$	others
K1		3.98	1.82, 1.76	$C^{\gamma}H$ 1.19, 1.19; $C^{\delta}H$ 1.64, 1.64; $C^{\epsilon}H$ 2.86, 2.86
T2		4.56	3.94	$C^{\gamma}H_3$ 1.10
Y3	9.07	4.54	2.96, 2.76	$C^{\delta}H$ 7.13; $C^{\epsilon}H$ 6.84
Q4	8.82	4.65	2.02, 1.94	$C^{\gamma}H$ 2.29, 2.14; $N^{\epsilon}H$ 8.0, 6.43
C5	8.93	4.40	3.54, 2.85	
Q6	9.13	4.26	1.72, 1.72	$C^{\gamma}H$ 1.59, 1.59; $N^{\epsilon}H$ 7.25, 6.79
Y7	9.63	4.55	2.61, 1.27	$C^{\gamma}H$ 6.95; $C^{\epsilon}H$ 6.80
C8	8.05	5.08	3.44, 3.24	
E9	8.63	4.26	2.16, 2.16	$C^{\gamma}H$ 2.16, 2.16
F10	8.89	4.16	2.88, 2.46	$C^{\delta}H$ 7.25; $C^{\epsilon}H$ 7.38; $C^{\zeta}H$ 7.38
R11	7.73	5.02	1.62, 1.48	$C^{\gamma}H$ 1.59, 1.42; $C^{\delta}H$ 3.11, 3.11; $N^{\epsilon}H$ 7.16
F12	8.73	4.82	2.76, 3.44	$C^{\delta}H$ 7.29; $C^{\epsilon}H$ 6.96; $C^{\zeta}H$ 6.38
A13	9.14	4.76	1.57	
D14	7.59	4.77	2.78, 2.78	
S15	8.42	3.37	3.62, 3.31	
S16	8.51	4.15	3.92, 3.92	
N17	8.35	4.41	2.94, 2.72	$N^{\delta}H$ 8.48, 7.18
L18	7.03	3.35	1.95, 1.28	$C^{\gamma}H$ 1.65; $C^{\delta}H_3$ 1.14, 1.05
K19	8.05	3.92	1.96, 1.96	$C^{\gamma}H$ 1.45, 1.45; $C^{\delta}H$ 1.69, 1.61; $C^{\epsilon}H$ 2.97, 2.97
T20	8.15	3.91	4.12	$C^{\gamma}H_3$ 1.24
H21	7.82	4.22	3.37, 2.89	$C^{\delta 2}H$ 7.47; $C^{\epsilon 2}H$ 7.65
I22	8.71	3.55	1.99	$C^{\gamma}H_3$ 1.08; $C^{\gamma}H$ 2.25, 1.54; $C^{\delta}H_3$ 1.23
K23	7.80	4.09	1.94, 1.94	$C^{\gamma}H$ 1.53, 1.46; $C^{\delta}H$ 1.69, 1.69; $C^{\epsilon}H$ 2.97, 2.97
T24	7.93	4.13	4.13	$C^{\gamma}H_3$ 1.26
K25	8.36	4.26	0.88, 0.69	$C^{\gamma}H$ 1.17, 1.08; $C^{\delta}H$ 1.50, 1.50; $C^{\epsilon}H$ 2.98, 2.98
H26	7.49	5.15	2.96, 2.72	$C^{\delta 2}H$ 6.73; $C^{\epsilon 2}H$ 7.60
S27	7.76	4.29	3.97, 3.97	
K28	8.21	4.42	1.89, 1.67	$C^{\gamma}H$ 1.36, 1.36; $C^{\delta}H$ 1.60, 1.60; $C^{\epsilon}H$ 2.92, 2.92
E29	8.10	4.24	1.93, 1.77	$C^{\gamma}H$ 2.13, 2.13
K30	7.94	4.15	1.83, 1.72	$C^{\gamma}H$ 1.40, 1.40; $C^{\delta}H$ 1.70, 1.70; $C^{\epsilon}H$ 3.02, 3.02

Table III: Chemical Shifts of Assigned ^{1}H-NMR Resonances in the [Tyr10Phe; Phe12Tyr] Analogue

residue	chemical shift (ppm)			
	NH	$C^{\alpha}H$	$C^{\beta}H$	others
K1		3.95	1.78, 1.73	$C^{\gamma}H$ 1.17, 1.17; $C^{\delta}H$ 1.61, 1.61; $C^{\epsilon}H$ 2.85, 2.85
T2	8.19	4.47	3.88	$C^{\gamma}H_3$ 1.03
Y3	8.92	4.48	2.89, 2.45	$C^{\delta}H$ 6.99; $C^{\epsilon}H$ 6.79
Q4	8.63	4.69	1.97, 1.89	$C^{\gamma}H$ 2.46, 2.14; $N^{\epsilon}H$ 7.99, 6.45
C5	9.00	4.32	3.51, 2.85	
Q6	9.01	4.23	1.68, 1.68	$C^{\gamma}H$ 1.61, 1.61; N^{H} 7.23, 6.86
Y7	9.67	4.57	2.63, 1.32	$C^{\delta}H$ 6.89; $C^{\epsilon}H$ 6.88
C8	7.98	5.03	3.38, 3.24	
E9	8.54	4.27	2.17, 2.11	$C^{\gamma}H$ 2.27, 2.27
F10	8.98	4.18	2.89, 2.43	$C^{\delta}H$ 7.14; $C^{\epsilon}H$ 7.28; $C^{\zeta}H$ 7.28
R11	7.59	5.08	1.59, 1.45	$C^{\gamma}H$ 1.57, 1.41; $C^{\delta}H$ 3.08, 3.08; $N^{\epsilon}H$ 7.12
Y12	8.55	4.69	3.25, 2.69	$C^{\delta}H$ 7.02; $C^{\epsilon}H$ 6.4
A13	8.92	4.87	1.54	
D14	7.67	4.87	2.81, 2.74	
S15	8.58	3.48	3.64, 3.35	
S16	8.61	4.16	3.91, 3.91	
N17	8.17	4.47	2.87, 2.60	$N^{\delta}H$ 8.39, 7.18
L18	7.04	3.81	1.90, 1.16	$C^{\gamma}H$ 1.69; $C^{\delta}H_3$ 1.14, 1.00
K19	8.04	3.93	1.94, 1.94	$C^{\gamma}H$ 1.42, 1.42; $C^{\delta}H$ 1.68, 1.61; $C^{\epsilon}H$ 2.95, 2.95
T20	7.99	3.89	4.13	$C^{\gamma}H_3$ 1.22
H21	7.77	4.18	3.52, 3.01	$C^{\delta 2}H$ 7.48; $C^{\epsilon 2}H$ 7.64
I22	8.79	3.51	1.97	$C^{\gamma}H_3$ 1.04; $C^{\gamma}H$ 2.18, 1.53, $C^{\delta}H_3$ 1.17
K23	7.77	4.04	1.92, 1.92	$C^{\gamma}H$ 1.47, 1.47; $C^{\delta}H$ 1.66, 1.66; $C^{\epsilon}H$ 2.94
T24	7.84	4.10	4.10	$C^{\gamma}H_3$ 1.22
K25	8.28	4.24	0.82, 0.68	$C^{\gamma}H$ 1.11, 1.04; $C^{\delta}H$ 1.47, 1.47; $C^{\epsilon}H$ 2.93, 2.93
H26	7.52	5.15	2.92, 2.64	$C^{\delta 2}H$ 6.76; $C^{\epsilon 2}H$ 8.07
S27	7.75	4.29	3.94, 3.94	
K28	8.28	4.40	1.86, 1.65	$C^{\gamma}H$ 1.34, 1.34; $C^{\delta}H$ 1.65, 1.57; $C^{\epsilon}H$ 2.93, 2.93
E29	8.09	4.21	1.97, 1.74	$C^{\gamma}H$ 2.09, 2.09
K30	7.90	4.14	1.81, 1.72	$C^{\gamma}H$ 1.38, 1.38; $C^{\delta}H$ 1.67, 1.67; $C^{\epsilon}H$ 3.00, 3.00

peptide. For each peptide the most consistent DG/SA model exhibited a maximum NOE restraint violation of ≤0.10 Å. For the two analogues root-mean-square deviations (rmsd) are shown by residue in Figure 5. Ramachandran plots are provided as supplementary material. In each ensemble the positions of residues 1 and 27–30 are not well-defined.

In DG/SA models the three peptides exhibit essentially identical main-chain conformations. In Figure 6A backbone ensembles of the [Tyr10Phe] (red) and [Tyr10Phe; Phe12Tyr] (blue) analogues are superimposed. The rmsd between the

Table IV: Differences in Chemical Shifts (ppm) of Selected Residues[a]

residue	NH	$C^{\alpha}H$	$C^{\beta}H$	other
			Set A	
Y3	−0.01	−0.04	0.00, −0.02	$C^{\delta}H_2$ 0.09; $C^{\epsilon}H_2$ 0.01
Q4	0.02	−0.04	−0.01, −0.01	$C^{\delta}H_2$ −0.01, −0.01; $N^{\epsilon}H_2$ 0.04, −0.01
C5	0.00	0.00	0.03, 0.00	
Q6	0.05	0.01	−0.01, −0.01	$C^{\delta}H_2$ −0.04, −0.04; $N^{\epsilon}H_2$ −0.04 −0.03
C8	−0.03	−0.01	−0.02, −0.02	
*10	0.04	0.07	0.04, 0.08	
F12	0.00	0.04	0.03, −0.01	$C^{\delta}H$ 0.00; $C^{\epsilon}H$ 0.02; $C^{\zeta}H$ 0.02
N17	0.07	0.05	0.00, 0.01	$N^{\delta}H_2$ 0.00, 0.07
L18	0.00	0.04	0.00, 0.00	$C^{\gamma}H$ −0.01; $C^{\delta}H_3$ 0.00, −0.01
H21	−0.02	−0.01	0.02, 0.00	$C^{\delta}H$ 0.06; $C^{\epsilon}H$ 0.05
I22	0.00	0.01	−0.01	$C^{\gamma'}H_3$ 0.00; $C^{\gamma}H$ −0.01, 0.00, $C^{\delta}H_3$ 0.00
			Set B	
Y3	**−0.15**	−0.06	0.06, **0.31**	$C^{\delta}H_2$ **−0.14**; $C^{\epsilon}H_2$ −0.05
Q4	**0.19**	−0.04	−0.05, −0.05	$C^{\delta}H_2$ **0.17**, 0.00; $N^{\epsilon}H_2$ −0.01, 0.02
C5	0.07	−0.08	0.03, 0.00	
Q6	**−0.12**	−0.03	−0.04, −0.04	$C^{\delta}H_2$ 0.02, 0.02; $N^{\epsilon}H_2$ 0.02, 0.07
C8	−0.07	−0.05	−0.06, 0.00	
F10	0.09	0.07	0.01, −0.03	$C^{\delta}H$ **−0.11**; $C^{\epsilon}H$ **−0.10**; $C^{\zeta}H$ **−0.10**
*12	**0.18**	**−0.13**	**−0.19**, −0.07	
N17	**−0.18**	0.06	−0.07, **−0.12**	$N^{\delta}H_2$ 0.00, 0.09
L18	0.01	**0.46**	−0.05, **−0.12**	$C^{\gamma}H$ 0.04; $C^{\delta}H_3$ 0.00, −0.05
H21	−0.05	−0.04	**0.25, 0.12**	$C^{\delta}H$ 0.01; $C^{\epsilon}H$ −0.01
I22	0.08	−0.04	−0.02	$C^{\gamma'}H_3$ −0.04; $C^{\gamma}H$ −0.07, −0.02, $C^{\delta}H_3$ −0.06

[a] Chemical-shift differences ≤−0.10 ppm or ≥0.10 ppm are shown in boldface. In set A are given differences between the [Y10F] analogue and the parent peptide; in set B are given corresponding differences between the [Y10F; F12Y] and [Y10F] analogues, respectively. Asterisks indicate sites of substitution.

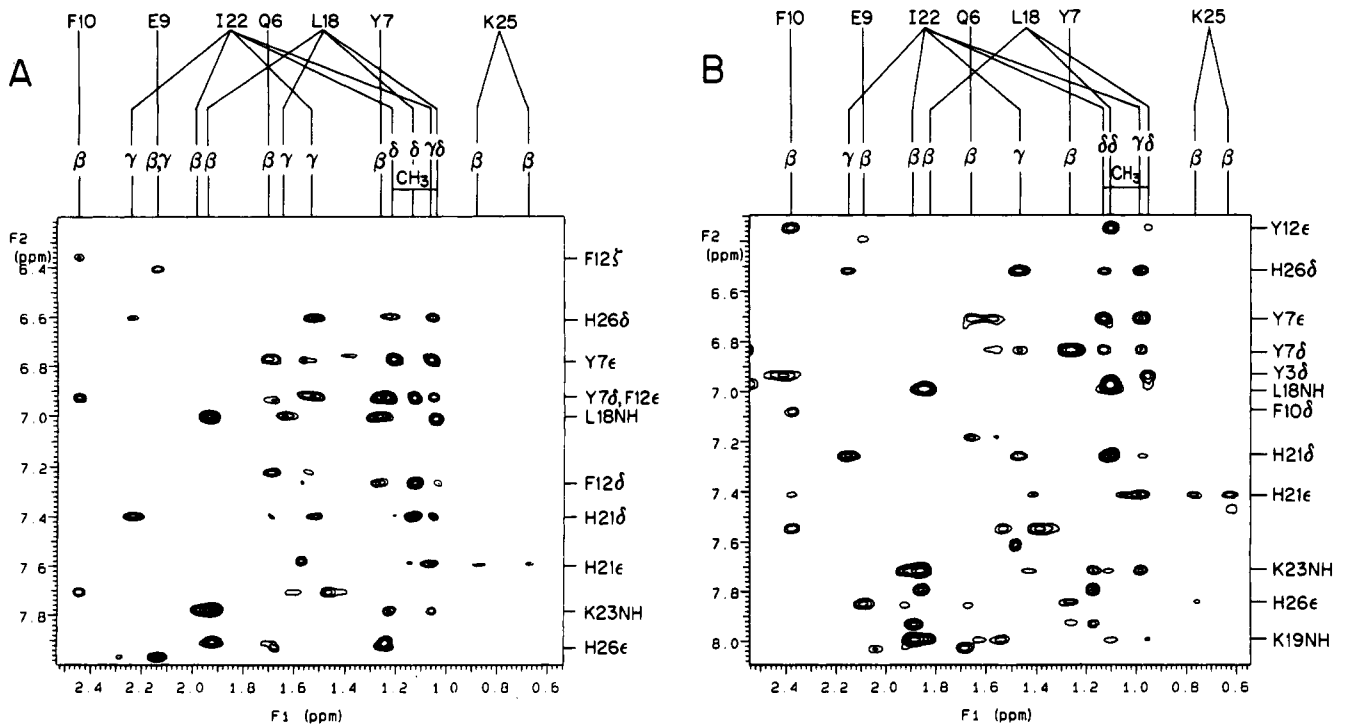

FIGURE 3: Long-range NOEs observed in the NOESY spectra of the [Tyr10Phe] (A) and [Tyr10Phe; Phe12Tyr] (B) analogues, respectively. The region shown contains contacts between aromatic and aliphatic protons (conditions: 25 °C, mixing time 200 ms, pH 6.0 in H_2O).

average backbone conformation of the parent peptide and [Tyr10Phe] analogue is 0.42 Å; between the parent peptide and [Tyr10Phe; Phe12Tyr] analogue, 1.18 Å; and between the two analogues, 1.3 Å. Such differences are commensurate with the imprecision of the individual ensembles (Figure 5) and limited ensemble sizes. In Figure 6B are shown the side chains of aromatic residues at positions 10 and 12 relative to Leu18, His21, and His26. Edge-to-face packing (Burley & Petsko, 1985, 1986) is observed in each case between the aromatic residue at position 12 and His 21 (red arrow). Nevertheless, the distance and orientation of the two aromatic–histidine interactions differ; their geometric relationships are described in Table VI using a polar coordinate system derived from Burley and Petsko (1988) [see also Jasanoff et al. (1992)].

In Figure 6C are shown the positions of Phe12 (red) and Tyr12 (blue) relative to the His21 ring. The observed shift in the configuration of Tyr12 is required (i) to satisfy novel NOE restraints from the β-resonances of Tyr12 to Tyr3-NH and (ii) to avoid steric overlap between the Tyr12 *p*-OH and the His21 imidazolic ring; such overlap occurs when a *p*-OH group is appended to Phe12 in the majority of structures of the parent peptide. Relative to Phe12, Tyr12 is displaced somewhat out of the hydrophobic core. In the [Tyr10Phe] ensemble the mean solvent accessibility (probe radius 1.6 Å)

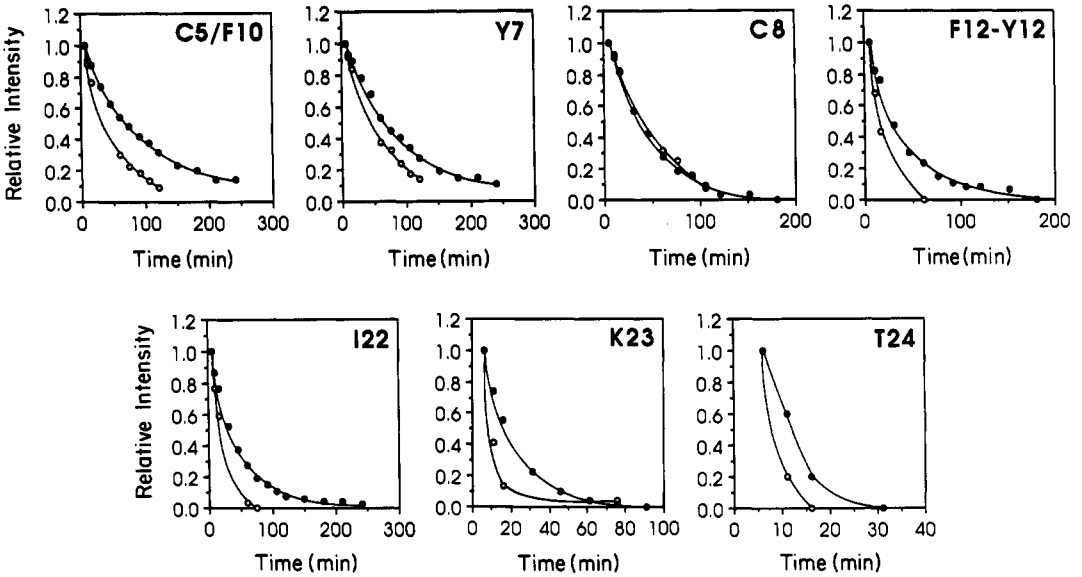

FIGURE 4: Time course of exchange in D_2O of the eight slowly exchanging amide resonances. In each panel [Tyr10Phe] and [Tyr10Phe; Phe12Tyr] analogues are indicated by filled and open circles, respectively. Exchange in the parent peptide is similar to that of the [Tyr10Phe] analogue (not shown). The NH resonances of Cys5 and residue 10 overlap in 1D spectra; however, comparison with other analogues (Qian & Weiss, 1992) indicates that the longer lived component is due to the NH of residue 10.

Table V: Summary of Experimental Restraints

	analogue		
	parent peptide	[Y10F]	[Y10F; F12Y]
NOEs			
total	241	243	205
sequential	119	119	97
medium range	57	57	47
long range	65	67	61
dihedral angles	28	33	26
hydrogen bonds	7	7	7

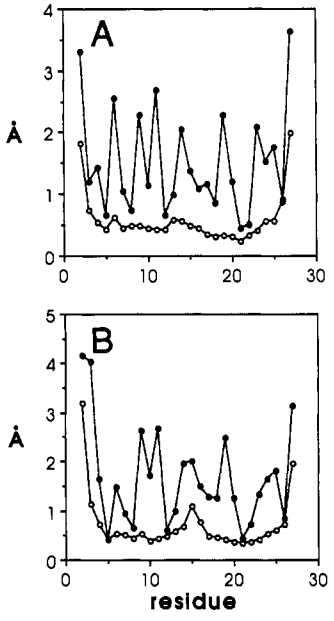

FIGURE 5: rms deviations shown by residue for main-chain (○) and side-chain atoms (●) of [Tyr10Phe] (A) and Tyr10Phe; Phe12Tyr] (B) analogues, respectively.

of the para proton of Phe12 is 0.5 Å^2 (standard deviation ±0.4 Å^2). In contrast, in the [Tyr10Phe; Phe12Tyr] ensemble the mean solvent accessibility of a correspondingly placed proton (i.e., in place of the Tyr *p*-OH group) is 6.1 Å^2 (standard deviation ±2.3 Å^2). The position of the Tyr12 *p*-OH is contiguous to the DNA-binding surface, as defined in the X-ray structure of the Zif268–DNA complex (Pavletich & Pabo, 1991).

Minor Conformation of the [Tyr10Phe; Phe12Tyr] Analogue. Additional DG/SA calculations were performed in which weak nonlocal NOEs from the Phe10 aromatic ring were added to the above restraint list. The resulting structures violated either or both Phe10- and Tyr12-related restraints. Structures with lowest restraint violation exhibited horizontal stacking of the Phe10 and Tyr12 rings; the models consistently predict strong NOEs between these rings, which are not observed. Such anomalous features presumably represent a nonphysical compromise between geometrically inconsistent restraints. These calculations highlight an intrinsic limitation to DG in the presence of conformational heterogeneity. Additional DG calculations were performed with Phe10-related NOEs included and Tyr12-related NOEs omitted. Residual restraint violations are low, in accord with the primary DG models above. These alternative structures exhibit displaced-horizontal packing between Phe10 and His21 as in ZFY-6T (Kochoyan et al., 1991a,b) and the Phe10–Ser12 analogue ZFY-Phe (Qian & Weiss, 1992); Tyr12 is excluded from the hydrophobic core. The latter calculations provide a plausible model of the minor conformer of the [Tyr10Phe; Phe12Tyr] analogue.

It was observed above that the [Tyr10Phe; Phe12Tyr] analogue—but not the [Tyr10Phe] analogue—exhibits significant perturbations in chemical shift (Table IV). Such perturbations have several possible origins, including the magnetic anisotropy of the Tyr12 *p*-OH (Osapay & Case, 1991) and structural changes in positions of aromatic rings (Johnson & Bovey, 1958). Since the presumed major and minor conformations are in fast exchange, structural features of either or both may contribute to average chemical shifts. In the major state displacement of Tyr12 would be expected to alter its ring-current contribution. In the minor state the ring-current contributions of both Y12 and an inward F10 would be expected to be altered. Indeed, the changes in chemical shift observed in the [Tyr10Phe; Phe12Tyr] analogue are in the direction of the secondary shifts of ZFY-6T (Kochoyan et al., 1991a).

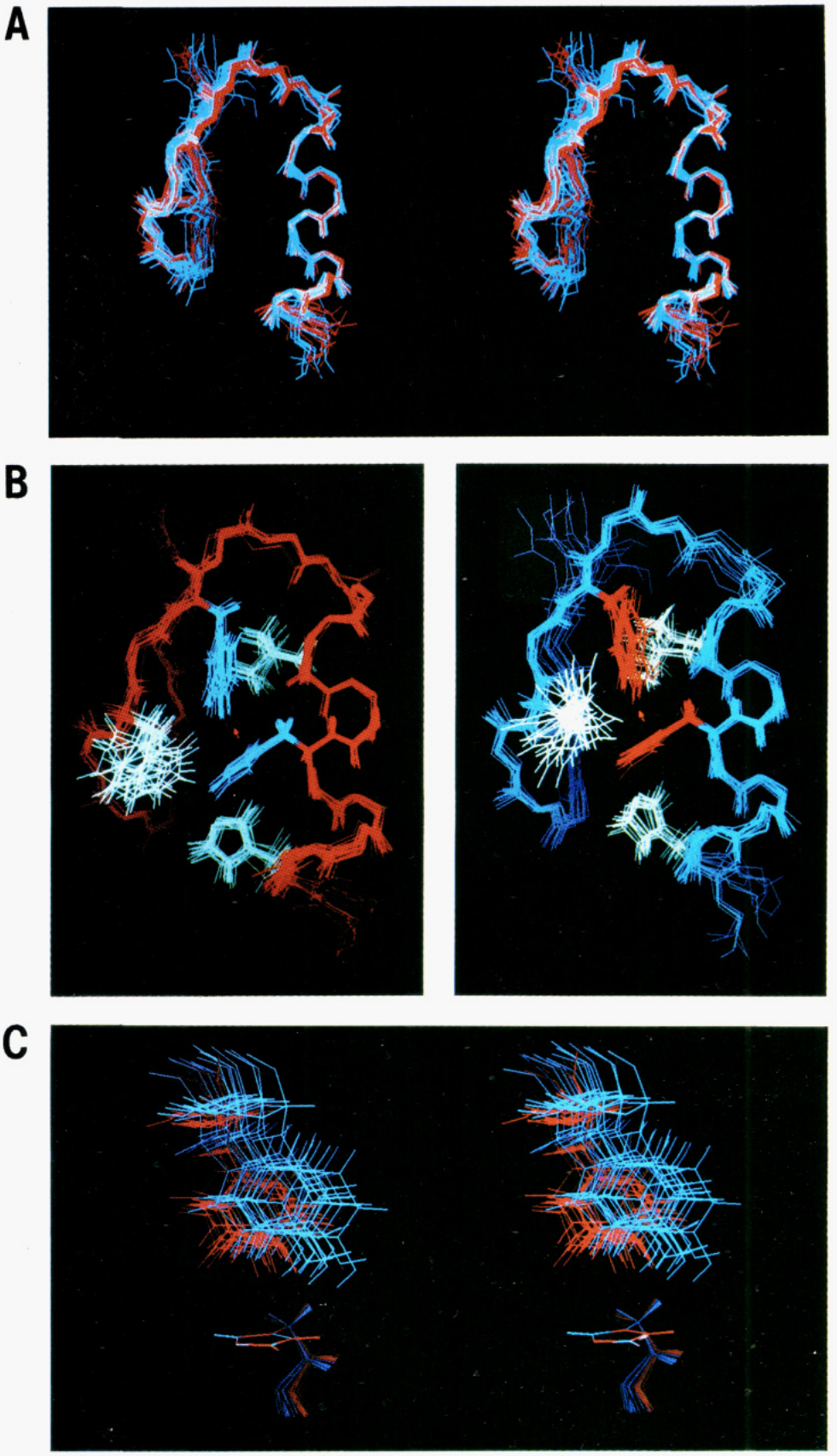

FIGURE 6: (A) DG/SA ensembles (main chain only) of the [Tyr10Phe] analogue (red) and the [Tyr10Phe; Phe12Tyr] analogue (blue). The chain appears white where red and blue colors overlap. The main-chain structures of the parent peptide (Jasanoff et al., 1992) and the two analogues are essentially identical. (B, left) DG/SA ensemble of the [Tyr10Phe] analogue. The backbone is shown in red; the side chains of Phe12 and His21 are in blue; and the side chains of Phe10, Leu18, and His26 are in white. The red arrow indicates Phe12. (B, right) DG/SA ensemble of the [Tyr10Phe; Phe12Tyr] analogue. The backbone is shown in blue; the side chains of Tyr12 and His21 are in red; and the side chains of Phe10, Leu18, and His26 are in white. The red arrow indicates Tyr12. (C) Positions of Phe12 (red) and Tyr12 (blue) relative to the imidazole ring of H21. In panels A and B the ensembles were aligned according to the main-chain atoms of residues 3–26; in panel C the ensembles were aligned according to the ring of HisB26.

Table VI: Aromatic–Histidine Interactions in ZFY Analogues[a]

analogue	r	θ	ϕ	D
(A) parent peptide[b]	5.0 ± 0.3[c]	153 ● 2	133 ● 11	47 ● 5
(B) [Y10F]	5.0 ± 0.3	156 ± 4	129 ± 12	49 ± 10
(C) [Y10F; F12Y]	5.5 ± 0.2	156 ± 9	153 ± 17	61 ● 4

[a] Polar coordinates used to describe Phe–His and Tyr–His pairs are as defined in Jasanoff et al. (1992). In each case the origin of the coordinate system is located in the center of the His21 ring, and the second ring is at position 12. [b] The parent peptide [designated ZFY-swivel in Jasanoff et al. (1992)] is related to ZFY-6T (Kochoyan et al., 1991) by an S12F substitution. [c] Errors are given as ±1 standard deviation from the mean.

DISCUSSION

The classical Zn finger (Ar-X-Cys-$X_{2,4}$-Cys-X_3-Phe-X_5-Leu-X_2-His-$X_{3,4}$-His) provides a model of a globular mini-domain whose folding properties may be investigated by peptide mutagenesis and ^{1}H-NMR spectroscopy (Parraga et al., 1988; Lee et al., 1989a,b; Omichinski et al., 1990, 1992; Neuhaus et al., 1990; Kochoyan et al., 1991a–d; Mortishire-Smith et al., 1991). Here we have focused on a conserved structural feature, edge-to-face packing of the central Phe and N-proximal histidine in the hydrophobic core. The solution structure of an analogue has been determined in which the Phe–His interaction is replaced by Tyr–His. Tyr-containing sequences are observed in a minority of Zn finger proteins (Gibson et al., 1988) and may be associated with a difference in mode of DNA binding. Our results demonstrate that a Phe → Tyr substitution leads to a small decrease in thermodynamic stability (as probed by pH-unfolding studies) and dynamic stability (as probed by amide proton exchange rates in D_2O). ^{1}H-NMR studies indicate that in the predominant conformer the $\beta\beta\alpha$ folding motif is retained with edge-to-face Tyr–His packing. Tyr–His packing differs in orientation, however, leading to partial displacement of the Tyr12 p-OH from the hydrophobic core. Such displacement avoids steric overlap with His21 and appears to alter a portion of the DNA-binding surface as defined by the Zif268 cocrystal structure (Pavletich & Pabo, 1991).

The present analogues also contain an aromatic residue at position 10. In ZFY-6T, which lacks an aromatic residue at position 12 (sequence Tyr_{10}-X-Ser_{12}), Tyr10 is stacked over His21 in the hydrophobic core (Kochoyan et al., 1991b). On introduction of a consensus aromatic residue (sequence Tyr_{10}-X-Phe_{12}), Tyr10 is excluded; its horizontal stacking with His21 is replaced by canonical Phe–His edge-to-face packing (Jasanoff et al., 1992). This analogue (ZFY-swivel; Table I) provided the starting point for the present study. We have shown that whereas the substitution Tyr10Phe is conservative in this context, the additional substitution Phe12Tyr exhibits dynamic instability and population of a minor conformer in which internal packing of residue 10 is restored. The conformational equilibrium presumably reflects competition between alternative aromatic–histidine interactions. Distance-geometry models of the major and minor conformers were calculated by inclusion or omission of related NOEs. This approach reflects our structural intuition. Structures calculated in the presence of inconsistent restraints represent a geometric compromise that is likely to be nonphysical. It will be of future interest to examine whether alternative algorithms, such as use of time-averaged restraints in restrained molecular dynamics (Torda et al., 1991), would provide plausible models of major and minor conformers independent of ad hoc intervention. Despite present limitations in the DG analysis, the NMR results clearly demonstrate that the Tyr12–His21 interaction is less strongly favored (relative to the alternative Phe10–His21 interaction) than that of Phe12–His21. In the absence of an aromatic residue at position 10, Tyr12-containing fingers are likely to adopt a unique conformation; such sequences are found in TFIIA (Brown et al., 1985) and Gli (Kinzler et al., 1988).

The isolated Zn finger provides an attractive model for analysis of protein folding because of its simplicity of sequence and richness of structure. The compression of folding information into a small subset of residues, as elegantly demonstrated by design of a minimalist peptide (Michael et al., 1992), provides an intriguing opportunity to dissect chemical contributions to domain stability, structure, and dynamics. Geometric differences between Phe–His and Tyr–His edge-to-face packing, as described in the present study, are likely to be general features of Zn finger architecture. Their functional consequences are not understood and in the future will be tested by complementary mutagenesis and crystallographic studies of variant Zn finger proteins. Model building based on the cocrystal structure of Zif268 (Pavletich & Pabo, 1991) makes interesting predictions. Analogous positioning of Tyr12 in the complex leads to partial steric overlap between its p-OH and a DNA phosphate. Such overlap is readily relieved by rigid-body repositioning of the finger in the major groove, which in turn permits formation of a novel hydrogen bond between the Tyr p-OH and the phosphate. Such repositioning could influence the detailed geometry of amino acid base contacts and thus extend the alphabet of a Zn finger–DNA recognition code (Desjarlais & Berg, 1992).

ACKNOWLEDGMENT

We thank C. E. Dahl for peptide synthesis; H. T. Keutmann for advice regarding peptide purification and sequencing; J. P. Lee and X. Qian for assistance with NMR measurements; D. A. Case and P. E. Wright for the coordinates of Xfin-31; N. Pavletich and C. O. Pabo for the coordinates of the Zif268–DNA complex; G. M. Clore and A. Gronenborn for the coordinates of other Zn fingers; T. F. Havel for the program DG-II and advice; A. T. Brunger and M. Nilges for X-PLOR and advice; C. Redfield for J-coupling simulation software; and S. K. Burley, E. Fraenkel, M. Kochoyan, and G. A. Petsko for helpful discussion. NMR spectra were obtained at the Harvard Medical School NMR Facility.

SUPPLEMENTARY MATERIAL AVAILABLE

Four figures showing 1D-NMR spectra of ZFY analogues, pH dependence of CD $[\theta]_{222}$, amide–aromatic regions of NOESY spectra, and Ramachandran plots and two tables of DG/SA restraints (15 pages). Ordering information is given on any current masthead page.

REFERENCES

Akke, M., Drakenberg, T., & Chazin, W. J. (1992) *Biochemistry 31*, 1011–1020.

Berg, J. M. (1988) *Proc. Natl. Acad. Sci. U.S.A. 85*, 99–487.

Berg, J. M. (1990) *Annu. Rev. Biophys. Biophys. Chem. 19*, 405–421.

Bowie, J. U., Reidhaar-Olson, J. F., Lim, W. A., & Sauer, R. T. (1990) *Science 247*, 1306–1310.

Brown, R. S., Sander, C., & Argos, P. (1985) *FEBS Lett. 186*, 271–274.

Burley, S. K., & Petsko, G. A. (1985) *Science 229*, 23–28.

Burley, S. K., & Petsko, G. A. (1986) *J. Am. Chem. Soc. 108*, 7995.

Burley, S. K., & Petsko, G. A. (1988) *Adv. Protein Chem. 39*, 125–189.
Desjarlais, J. R., & Berg, J. M. (1992) *Proc. Natl. Acad. Sci. U.S.A. 89*, 7345–7349.
Frankel, A. D., Berg, J. M., & Pabo, C. O. (1987) *Proc. Natl. Acad. Sci. U.S.A. 84*, 4841–4845.
Gibson, T. J., Postma, J. P. M., Brown, R. S., & Argos, P. (1988) *Protein Eng. 2*, 209–218.
Jasanoff, A., Kochoyan, M., Fraenkel, E., Lee, J. P., & Weiss, M. A. (1992) *J. Mol. Biol. 225*, 1035–1047.
Johnson, C. E., & Bovey, F. A. (1958) *J. Chem. Phys. 29*, 1012–1017.
Karlstrom, G., Linse, P., Wallqvist, A., & Jonsson, B. (1983) *J. Am. Chem. Soc. 105*, 3776–3782.
Kinzler, K. W., Ruppert, J. M., Bigner, S. H., & Vogelstein, B. (1988) *Nature 332*, 371–374.
Klevit, R. E. (1991) *Science 253*, 1367.
Klevit, R. E., Herriol, J. R., & Horvath, S. (1990) *Proteins 7*, 214–226.
Klug, A., & Rhodes, D. (1987) *Trends Biochem. Sci. 12*, 464–468.
Kochoyan, M., Havel, T. F., Nguyen, D., Dahl, C. E., Keutmann, H. T., & Weiss, M. A. (1991a) *Biochemistry 30*, 3371–3386.
Kochoyan, M., Keutmann, H. T., & Weiss, M. A. (1991b) *Biochemistry 30*, 7063–7072.
Kochoyan, M., Keutmann, H. T., & Weiss, M. A. (1991c) *Proc. Natl. Acad. Sci. U.S.A. 88*, 8455–8459.
Kochoyan, M., Keutmann, H. T., & Weiss, M. A. (1991d) *Biochemistry 30*, 9396–9402.
Lee, M. S., Gippert, G. P., Soman, K. V., Case, D. A., & Wright, P. E. (1989a) *Science 245*, 635–637.
Lee, M. S., Cavanagh, J., & Wright, P. E. (1989b) *FEBS Lett. 254*, 159–164.
Loewenthal, R., Sancho, J., & Fersht, A. R. (1992) *J. Mol. Biol. 224*, 759–770.
Michael, S. F., Kilfoil, V. J., Schmidt, M. H., Amann, B. T., & Berg, J. M. (1992) *Proc. Natl. Acad. Sci. U.S.A. 89*, 4796–4800.
Mortishire-Smith, R. J., Lee, M. S., Bolinger, L., & Wright, P. E. (1992) *FEBS Lett. 1*, 11–15.
Nardelli, J., Gibson, T. J., Vesque, C., & Charnay, P. (1991) *Nature 349*, 175–178.
Neuhaus, D., Nakaseko, Y., Nagai, K., & Klug, A. (1990) *FEBS Lett. 262*, 179–184.
Omichinski, J. G., Clore, G. M., Apella, E., Sakaguchi, K., & Gronenborn, A. M. (1990) *Biochemistry 29*, 9324–9334.
Osapay, K., & Case, D. A. (1991) *J. Am. Chem. Soc. 113*, 9436–9443.
Page, D. C., Mosher, R., Simpson, E., Fisher, E. M. C., Mardon, G., Pollack, J., McGillivray, B., de la Chapelle, A., & Brown, L. G. (1987) *Cell 51*, 1091–1104.
Parraga, G., Horvath, S. J., Eisen, A., Taylor, W. E., Hood, L., Young, E. T., & Klevit, R. E. (1988) *Science 241*, 1489–1492.
Pavletich, N. P., & Pabo, C. O. (1991) *Science 252*, 809–817.
Pollack, J., McGillivray, B., de la Chapelle, A., & Brown, L. G. (1987) *Cell 51*, 1091–1104.
Qian, X., & Weiss, M. A. (1992) *Biochemistry 31*, 7463–7476.
Redfield, C., & Dobson, C. M. (1990) *Biochemistry 29*, 7201.
Richardson, J. S., & Richardson, D. C. (1988) *Science 240*, 1648–1652.
Sandberg, W. S., & Terwilliger, T. C. (1991) *Proc. Natl. Acad. Sci. U.S.A. 88*, 1706–1710.
Smith, L. J., Sutcliffe, M. J., Redfield, C., & Dobson, C. M. (1991) *Biochemistry 30*, 986–996.
Torda, A. E., Sheek, R. M., & van Gunsteren, W. F. (1990) *J. Mol. Biol. 14*, 223–235.
Wagner, G., Braun, W., Havel, T. F., Shaumann, T., Go, N., & Wuthrich, K. (1987) *J. Mol. Biol. 196*, 611–633.
Weiss, M. A., & Keutmann, H. T. (1990) *Biochemistry 29*, 9808–9813.
Weiss, M. A., Mason, K. A., Dahl, C. E., & Keutmann, H. T. (1990) *Biochemistry 29*, 5660–5664.
Wuthrich, K. (1986) *NMR of Proteins and Nucleic Acids*, Wiley, New York.
Xu, R. X., Horvath, S. J., & Klevit, R. E. (1991) *Biochemistry 30*, 3365–3371.